Chem

CellPress

Article

Pillar[6]MaxQ: A potent supramolecular host for *in vivo* sequestration of methamphetamine and fentanyl

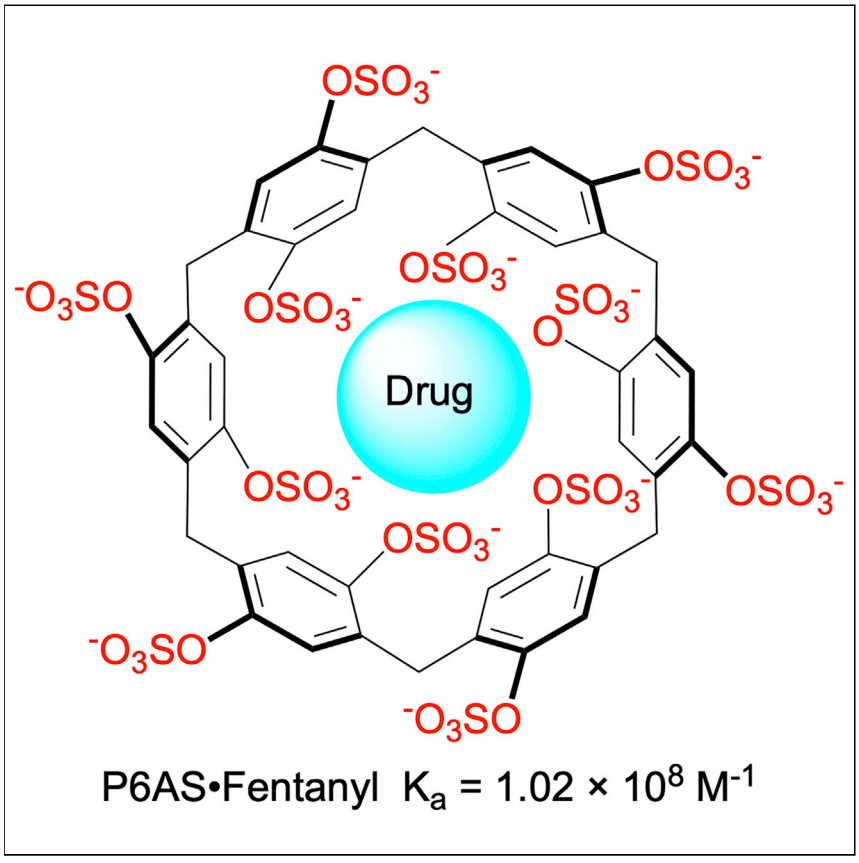

The physical, chemical, and even biological properties of guest compounds are altered when they are sequestered inside macrocyclic hosts. Pillar[6]MaxQ is a macrocyclic host that displays high *in vitro* binding affinity toward drugs of abuse in water. Pillar[6]MaxQ displays good biocompatibility according to a variety of *in vitro* and *in vivo* assays. The hyperlocomotion of mice treated with methamphetamine or fentanyl can be suppressed by treatment with Pillar[6]MaxQ from 5 to 15 min later.

Adam T. Brockett, Weijian Xue, David King, ..., Volker Briken, Matthew R. Roesch, Lyle Isaacs

lisaacs@umd.edu

Highlights

Pillar[6]MaxQ binds tightly to fentanyl, meth, PCP, MDMA, and mephedrone in water

Pillar[6]MaxQ displays good biocompatibility according to *in vitro* and *in vivo* assays

The *in vivo* hyperlocomotive effects of meth (fentanyl) can be reversed by Pillar[6]MaxQ

Pillar[6]MaxQ has significant potential as a broad-spectrum *in vivo* sequestrant

Brockett et al., Chem 9, 881–900
April 13, 2023
https://doi.org/10.1016/j.chempr.2022.11.019

Chem

CellPress

Article

Pillar[6]MaxQ: A potent supramolecular host for *in vivo* sequestration of methamphetamine and fentanyl

Adam T. Brockett,[1,4] Weijian Xue,[2,4] David King,[2] Chun-Lin Deng,[2] Canjia Zhai,[2] Michael Shuster,[3] Shivangi Rastogi,[3] Volker Briken,[3] Matthew R. Roesch,[1] and Lyle Isaacs[2,5,6,*]

SUMMARY

Pillar[6]MaxQ (P6AS) functions as an *in vivo* sequestration agent for methamphetamine and fentanyl. We use ^{1}H NMR, isothermal titration calorimetry, and molecular modeling to deduce the geometry and strength of the P6AS-drug complexes. P6AS forms tight complexes with fentanyl (K_d = 9.8 nM), PCP (17.1 nM), MDMA (25.5 nM), mephedrone (52.4 nM), and methamphetamine (101 nM). P6AS has good *in vitro* biocompatibility according to MTS metabolic, adenylate kinase cell death, and hERG ion channel inhibition assays, and the Ames fluctuation test. The no observed adverse effect level for P6AS is 45 mg/kg. The hyperlocomotion of mice treated with methamphetamine (0.5 mg/kg) can be ameliorated by treatment with P6AS (35.7 mg/kg) 5 min later, whereas the hyperlocomotion of mice treated with fentanyl (0.1 mg/kg) can be controlled by treatment with P6AS (5 mg/kg) up to 15 min later. P6AS has significant potential for development as a broad-spectrum *in vivo* sequestration agent.

INTRODUCTION

In recent years, there has been a dramatic increase in deaths associated with the abuse and overdose of prescription and illicit drugs (70,630 in 2019) in the United States, especially opioids like fentanyl and the stimulant methamphetamine.[1] It is estimated that 10.2% of the US population over 12 years of age used illicit drugs in the past month and that the healthcare costs and decreases in work productivity associated with drug abuse exceeds $271 billion per year.[2,3] Commonly abused substances include opioids (e.g., heroin, oxycodone, and fentanyl), stimulants (e.g., methamphetamine and cocaine), hallucinogens (ketamine, phencyclidine [PCP], and 3,4-methylenedioxy-methamphetamine [MDMA]), alcohol, marijuana, and prescription medicines. There is a societal need to develop new and improved therapeutics that are effective against the full range of drugs of abuse. Currently, opioid overdoses can be treated with the small molecule naloxone (NLX) which exerts its effect by a pharmacodynamic (PD) effect at the opioid receptor.[4] For high potency opioids like fentanyl and carfentanil multiple doses of naloxone (NLX) can be required and re-narcotization can occur.[5,6] Unfortunately, patients who have overdosed on non-opioids such as methamphetamine, cocaine, PCP, or ketamine cannot be saved by treatment with NLX. Pharmacokinetic (PK) approaches—which seek to reduce the concentration of freely circulating drug by catalytic destruction or non-covalent sequestration—are also being explored as therapies to treat drug overdose and abuse.[4] Human butyryl choline esterase, for example, hydrolyzes cocaine to ecgonine methyl ester and is investigated as a therapeutic for intoxication with

THE BIGGER PICTURE

Pillar[6]MaxQ displays high affinity for hydrophobic (di) cations. Drugs of abuse (opioids and non-opioids) are an important class of hydrophobic cations. Whereas opioid overdose (e.g., heroin) can be counteracted by naloxone, there are no specific antidotes for overdose with non-opioids (e.g., methamphetamine, PCP, and cocaine). Pillar[6]MaxQ forms tight complexes with fentanyl, PCP, MDMA, mephedrone, and methamphetamine in water according to isothermal titration calorimetry. We envisioned that *in vivo* sequestration of a drug as the Pillar[6]MaxQ-drug complex would turn off its biological activity. Pillar[6]MaxQ displays good *in vitro* and *in vivo* biocompatibility. Mice treated with methamphetamine or fentanyl display hyperlocomotion. Subsequent treatment (5–15 min later) of the mice with Pillar[6]MaxQ reduces their locomotion to baseline levels due to *in vivo* drug sequestration. Pillar[6]MaxQ is poised for further development as a broad-spectrum antidote for drugs of abuse.

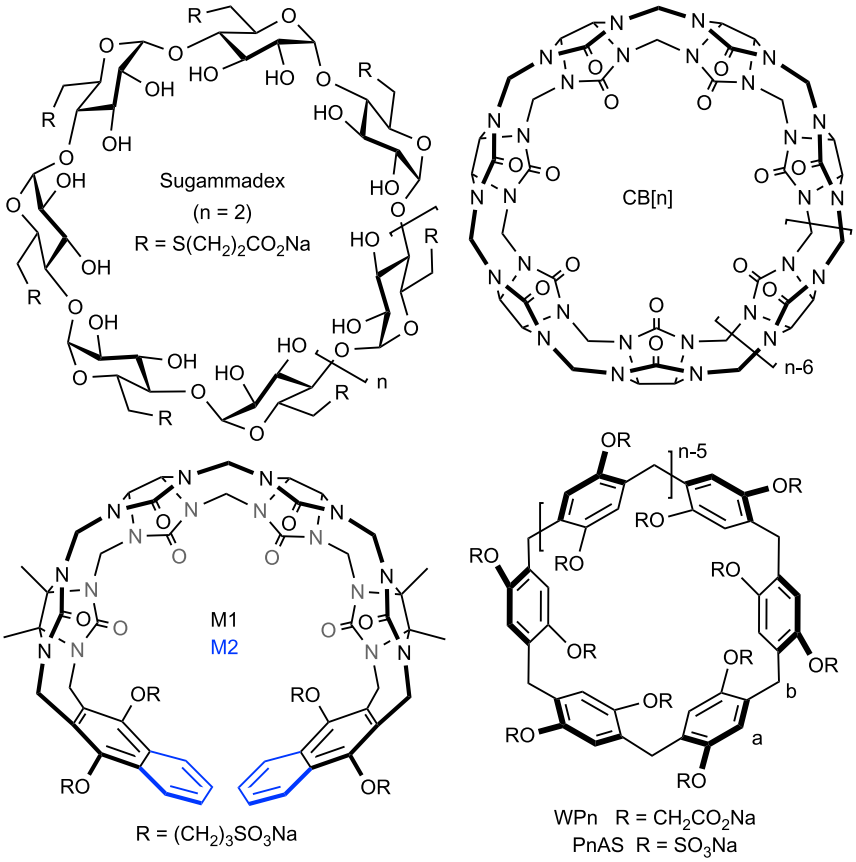

Figure 1. Chemical structures of Sugammadex, CB[n], acyclic CB[n]-type receptors (M1 and M2), and pillararenes

cocaine.[7–9] A variety of antibodies that bind tightly to cocaine, methamphetamine, fentanyl, and carfentanil have been created and demonstrated to have the ability to bind drugs in the bloodstream and prevent their passage across the blood brain barrier.[10–14] On the other hand, as supramolecular chemists, we envisioned that hosts that form tight host-drug complexes could be used to combat drug overdose by sequestering drugs via a supramolecular PK approach (Figure 1).[15,16]

Focal points of research in supramolecular chemistry include deepening our fundamental understanding of non-covalent interactions, the creation of new supramolecular systems, and ultimately their use in new chemical and biological applications.[17–20] Preorganized hosts are prized supramolecular building blocks because they often display high affinity and highly selective interactions with their guests.[17] Popular classes of hosts include cyclodextrins, calixarenes, cyclophanes, cavitands, cucurbiturils, and most recently pillararenes (Figure 1).[21–29] The chemical properties of free guests are often distinct from those of the host-guest complex that can be used to enable applications like chemical sensing, molecular machines, and supramolecular materials.[30–33] For hosts that are both soluble in water and biocompatible, application as components of imaging and drug delivery systems are popular.[34–38] For example, hydroxypropyl-β-CD and sulfobutylether-β-CD are used as solubilizing excipients for insoluble drugs that are currently approved for use in humans.[39] For hosts that display high affinity toward biologically active compounds in water, application as *in vivo* sequestration agents become feasible.[15,16]

[1]Department of Psychology and Program in Neuroscience and Cognitive Science (NACS), University of Maryland, College Park, MD 20742, USA

[2]Department of Chemistry and Biochemistry, University of Maryland, College Park, MD 20742, USA

[3]Department of Cell Biology and Molecular Genetics, University of Maryland, College Park, MD 20742, USA

[4]These authors contributed equally

[5]Twitter: @LyleIsaacsUMD

[6]Lead contact

*Correspondence: lisaacs@umd.edu

https://doi.org/10.1016/j.chempr.2022.11.019

For example, the γ-cyclodextrin derivative Sugammadex (Figure 1) is used clinically as a post-surgical reversal agent for the lingering effects of the neuromuscular blocking agents rocuronium and vecuronium.[40,41] Sugammadex is marketed by Merck as Bridion and had worldwide sales of $1.532 billion in 2021.

Stimulated by the stunning application of Sugammadex, we and others have been creating and using tight binding hosts for *in vivo* sequestration applications.[15,16] For example, Liu and co-workers showed that sulfo calix[4]arene displays high affinity toward paraquat and could be used as an *in vivo* antidote to alleviate the toxic effects of paraquat poisoning in mice.[42] The cucurbit[n]uril (CB[n]) family is well known for its ultratight binding properties in water.[43–45] Accordingly, the Wang group showed that CB[7] could be used to counteract the effects of paraquat (mice), to reverse paralysis induced by succinyl choline (mice), and to reverse general anesthesia (zebrafish), and we showed that a derivative of CB[8] could sequester PCP *in vivo* (mice).[46–49] We have synthesized acyclic CB[n]-type receptors (e.g., M1 and M2, Figure 1) and used them as *in vivo* sequestrants for neuromuscular blockers, anesthetics, and most recently drugs of abuse (e.g., methamphetamine and fentanyl).[50–52] In the past decade, pillararenes (e.g., WPn, Figure 1) have risen to prominence in supramolecular chemistry.[26,28,53] WP6 has been shown to act as an *in vivo* reversal agent for decamethonium, paraquat, and succinyl choline (mice).[48,54,55] Recently, we discovered that sulfated pillararenes (e.g., Pillar[*n*]MaxQ, a.k.a. P*n*AS, Figure 1) are ultratight binding hosts for hydrophobic (di)cations in aqueous solution.[56] In this paper, we present our investigation of the binding of WP6 and P*n*AS toward a panel of drugs of abuse (Figure 2), studies of the biocompatibility of P6AS, and *in vivo* efficacy studies demonstrating the ability of P6AS to reverse the hyperlocomotive effects of methamphetamine and fentanyl in mice. We selected methamphetamine and fentanyl for these *in vivo* efficacy studies—despite the observed tight binding P6AS toward MDMA, mephedrone, and PCP—because methamphetamine and fentanyl currently constitute the major public health threats in the United States.[1,57]

RESULTS AND DISCUSSION

This results and discussion section is subdivided as follows. First, we describe an improved purification method for larger scale synthesis of P6AS. Second, we present a qualitative investigation of host-drug binding by ^{1}H NMR spectroscopy followed by quantitative measurement of host-drug binding thermodynamics by isothermal titration calorimetry (ITC). Next, we present the results of a variety of *in vitro* and *in vivo* biocompatibility assays (metabolic and cell death assays, maximum tolerated dose (MTD), human ether-a-go-go related gene (hERG) ion channel, Ames fluctuation test). Finally, the efficacy of P6AS to sequester methamphetamine and fentanyl *in vivo* (mice) and ameliorate the observed hyperlocomotion is described.

Improved synthesis of P6AS

Our initial report on P6AS[56] described the small scale synthesis and purification of P6AS (352 mg), which required a time consuming and scale limiting desalting step by size exclusion chromatography (Sephedex G25). Before proceeding toward the *in vivo* application of P6AS we sought to improve the desalting step. We found that the synthesis of P6AS could be successfully scaled up to yield 7.3 g P6AS in a single reaction. The desalting process was substantially improved based on the differential solubility of P6AS and the inorganic salts in mixtures of EtOH and H_2O and separately in acetone and H_2O as described in the supplemental information.

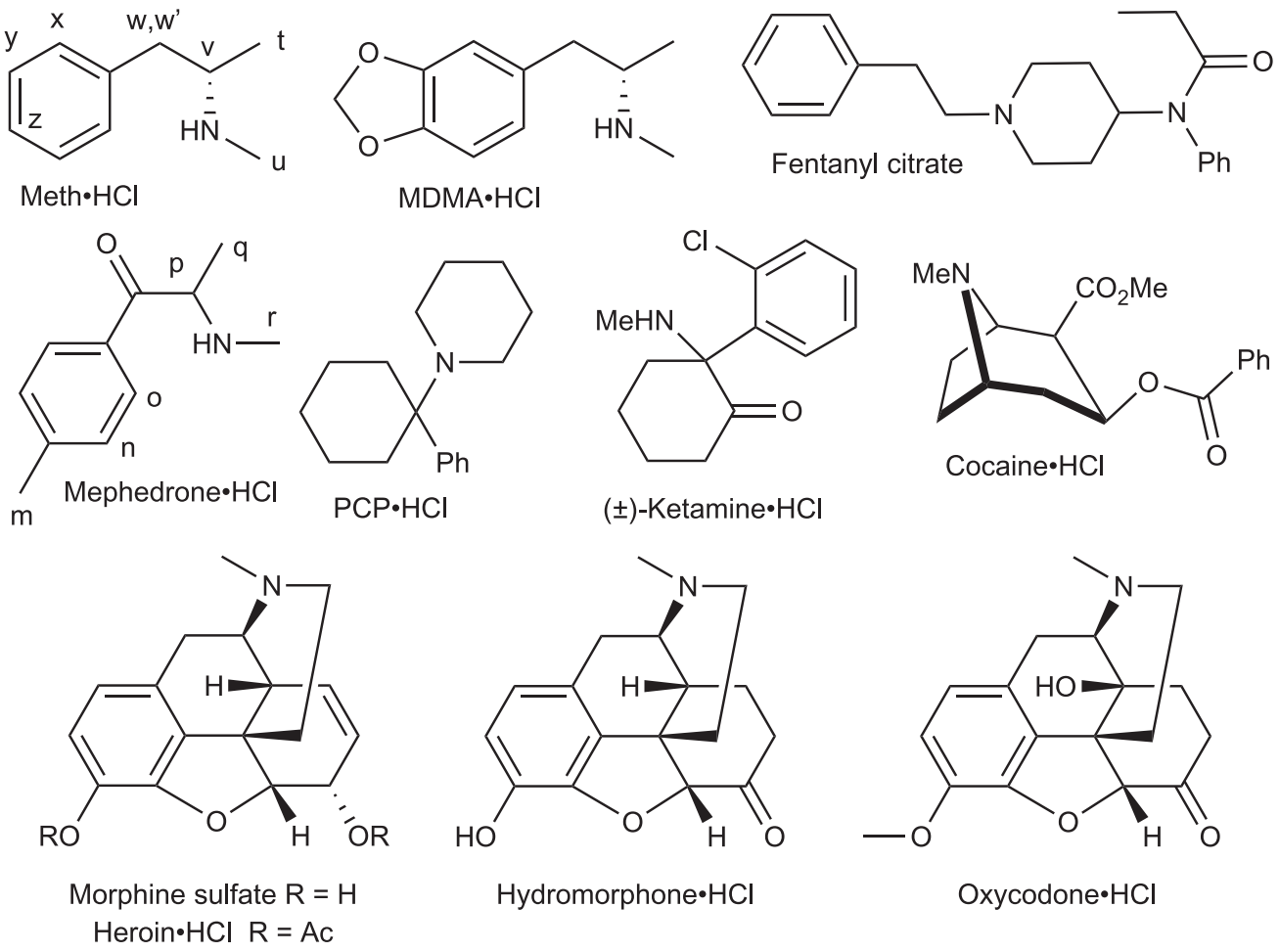

Figure 2. Chemical structures of drugs studied in this paper

Qualitative study of host-drug binding by ^{1}H NMR spectroscopy

Initially, we performed a qualitative study of the host-drug binding by ^{1}H NMR spectroscopy at different host:drug molar ratios to glean information about host-drug complex geometry and binding dynamics. Figures 3A and 3B shows the ^{1}H NMR spectra recorded for uncomplexed P6AS and methamphetamine (meth) whereas Figures 3C and 3D show the spectra for 1:1 and 1:2 mixtures of P6AS and meth. Upon formation of the P6AS-meth complex, the resonances for the protons on the aromatic ring (H_x, H_y, H_z) and the alkyl region (H_v, $H_{w,w'}$, H_t) undergo significant upfield changes in chemical shift whereas the NMe group (H_u) displays only small upfield shifts. These observations indicate that the hydrophobic phenylethyl ammonium ion region is buried within the anisotropic magnetic shielding environment of the P6AS cavity and the NMe group is located outside the cavity.[28] At a 1:2 P6AS:meth ratio, the resonances for meth shift back toward the chemical shifts observed for uncomplexed meth, which indicates that the guest exchange process is fast with respect to the chemical shift timescale. Figures 3E–3G show the spectra recorded for mephedrone and 1:1 and 1:2 mixtures of mephedrone with P6AS. Similar to methamphetamine, the mephedrone aromatic ring protons (H_n, H_o), methine H_p and methyl group H_q undergo significant upfield shifts indicating they are located inside the P6AS cavity within the P6AS-mephedrone complex. At a 2:1 mephedrone:P6AS ratio, the resonances shift back toward the chemical shift for

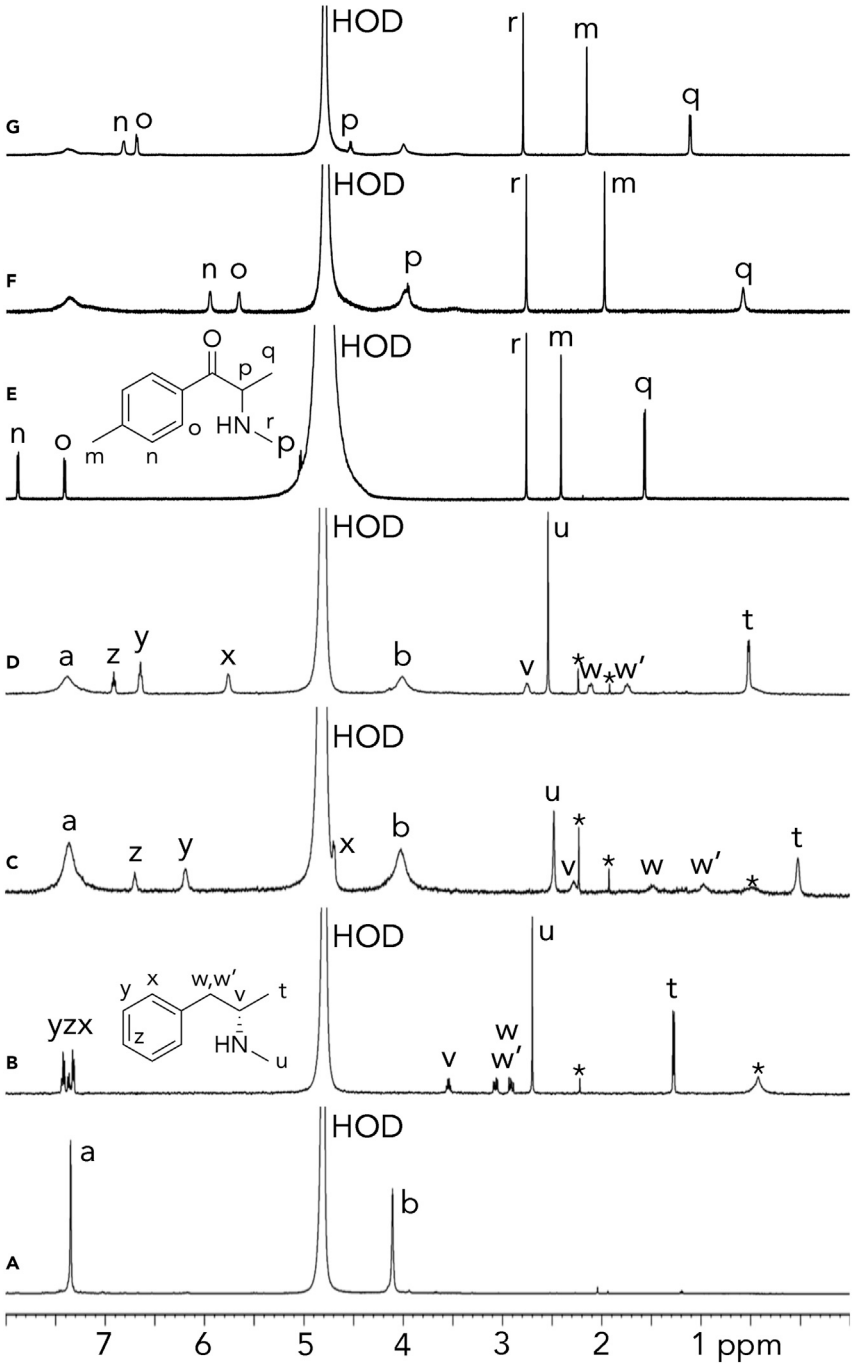

Figure 3. ^{1}H NMR spectra recorded (500 MHz, RT, 20 mM phosphate-buffered D_2O) for P6AS-drug complexes

(A) P6AS (2 mM), (B) methamphetamine (2 mM), (C) an equimolar mixture of P6AS and methamphetamine (0.5 mM), (D) a 2:1 mixture of methamphetamine (1 mM) and P6AS (0.5 mM), (E) mephedrone (1 mM), (F) an equimolar mixture of P6AS and mephedrone (0.5 mM), and (G) a 2:1 mixture of mephedrone (1 mM) and P6AS (0.5 mM).

uncomplexed mephedrone, which indicates that exchange is fast on the chemical shift timescale. Related ^{1}H NMR stack plots were constructed for the remaining drugs with P6AS (supplemental information; Figures S1–S15), which display

substantial broadening of their resonances that complicates elucidation of the geometry of the other P6AS-drug complexes by analysis of ^{1}H NMR complexation induced changes in chemical shift. Accordingly, we performed molecular modeling using the Merck Molecular Force Field (MMFF) of all of the P6AS-drug complexes and the three-dimensional structures are given in the supplemental information (Figures S60–S71). For the narrower drugs (methamphetamine, fentanyl, mephedrone, and MDMA), we find that the hydrophobic arylethyl ammonium ion fully inserts into the hydrophobic cavity of P6AS assisted by the formation of direct ammonium●●●sulfate H-bonds. For the somewhat bulkier drugs (PCP, ketamine, and cocaine) only a portion of the hydrophobic residue (e.g., Ar ring) is capable of insertion into the aromatic cavity, once again assisted by ammonium●●●sulfate H-bonds. Finally, P6AS can only accommodate the bulkiest drugs (heroin, morphine, hydromorphone, and oxycodone) featuring the morphinan ring system by tilting one of the aromatic walls which opens the cavity and allows the NHMe group to enter the cavity which forms one ammonium●●●sulfate H-bond.

Determination of the thermodynamic parameters for host-guest complexation by ITC

After obtaining qualitative evidence that P6AS forms complexes with the drugs of abuse panel, we decided to measure the thermodynamics of host-drug binding for a series of hosts (P5AS, WP6, P6AS, and P7AS). We elected to perform these titrations in 20-mM sodium phosphate-buffered H_2O at pH 7.4 to allow comparison with the results obtained previously for acyclic CB[n]-type receptors (M1 and M2).[50,58] Given the tight binding of WP6 and P6AS toward organic (di) ammonium ion guests reported previously,[56,59,60] we decided to use ITC which is capable of accurately determining K_a values up to $\approx 10^7$ M^{-1} by direct ITC titrations and higher K_a values by competitive ITC titrations.[61–63] For all of the complexes of P5AS and WP6 and most of the complexes of P6AS and P7AS, direct titrations were possible. For example, the data obtained from the titration of a solution of WP6 (100 μM) in the ITC cell with fentanyl (1 mM) in the ITC syringe could be fitted to a 1:1 binding model by the PEAQ data analysis software with K_a = (1.69 ± 0.06) × 10^6 M^{-1} and ΔH = −11.9 ± 0.051 kcal mol^{-1} (supplemental information; Figure S23). For the tighter complexes formed between P6AS and methamphetamine, fentanyl, PCP, and MDMA, we turned to competitive ITC titrations. In competitive ITC titrations a solution of host and an excess of weaker binding guest whose K_a and ΔH values are known is titrated with the stronger binding guest from the ITC syringe; the data can then be fitted to a competition binding model to extract the K_a and ΔH values of the stronger binding guest.[63] Figure 4A shows a plot of the heat evolved versus time when a solution of P6AS (100 μM) and 1,3-propanediammonium dichloride (1 mM) in the cell was titrated with fentanyl (1 mM) in the ITC syringe. Figure 4B shows a plot of ΔH versus molar ratio which was fitted to the competition binding model using the known parameters for P6AS·1,3-propanediammonium (K_a = (5.18 ± 0.15) × 10^5 M^{-1}; −5.51 ± 0.028 kcal mol^{-1})[56] as inputs to determine the thermodynamic parameters for the P6AS·fentanyl complex (K_a = (1.02 ± 0.03) × 10^8 M^{-1}; ΔH = −15.0 ± 0.052 kcal mol^{-1}). The thermodynamic parameters for the remaining host-drug complexes were measured similarly (supplemental information; Figures S16–S22 and S24–S52), and the results are summarized in Table 1. The stoichiometry of the host-drug complexes were 1:1 as determined by the ITC N value unless noted otherwise. As a prelude to the *in vivo* work, we also measured the binding constants for P6AS-methamphetamine (K_a = 2.17 ± 0.22) × 10^6 M^{-1}; ΔH = −8.53 ± 0.08 kcal mol^{-1}) and P6AS-fentanyl (K_a = 1.28 ± 0.057) × 10^7 M^{-1}; ΔH = −14.9 ± 0.054 kcal mol^{-1}) in normal phosphate-buffered saline (PBS) by direct ITC titrations (supplemental information; Figures S31 and S33).

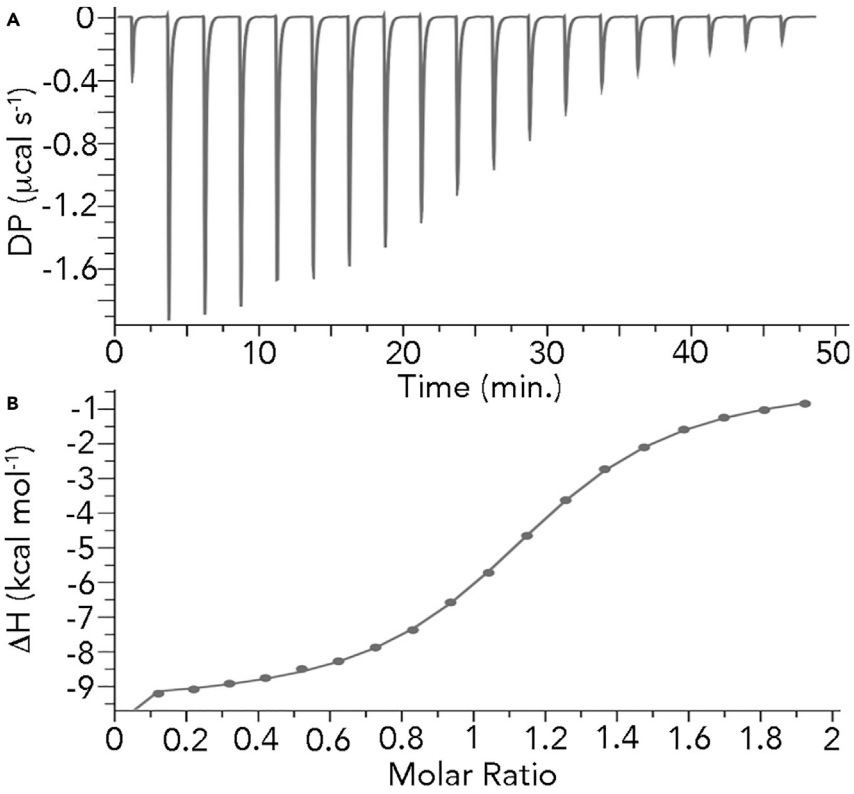

Figure 4. Competition ITC data used to measure K_a for P6AS-fentanyl

(A) Plot of DP versus time from the titration of P6AS (100 µM) and 1,3-propanediammonium dichloride (1.00 mM) with fentanyl (1.00 mM) in 20-mM sodium phosphate-buffered H_2O (pH 7.4). (B) Plot of the ΔH as a function of molar ratio. The solid line represents the best non-linear fit of the data to a competition binding model (K_a = [1.02 ± 0.03] × 10^8 M^{-1}, ΔH = −15.0 ± 0.052 kcal/mol, −TΔS = 4.02 kcal/mol).

Discussion of the thermodynamic parameters

The binding affinities measured for the P6AS-drug complexes span the range from 85,500 to 1.02 × 10^8 M^{-1}. As shown in Table 1, in several cases the titration of host (P5AS, WP6, or P7AS; 100 µM) with drug (1 mM) did not result in significant heat evolution which indicates low binding affinity ($K_a \leq 10^4$ M^{-1}). We did not work at the higher host concentrations (1 mM) needed to measure lower K_a values to minimize the quantity and concentrations of toxic drug substances used. All of the host-drug complexes are driven by large and negative enthalpies of complexation (ΔH [kcal mol^{-1}] for P5AS: −6.74 to −14.2; WP6: −7.75 to −15.5; P6AS: −8.62 to −22.0; P7AS: −6.86 to −18.1). Accordingly, the aqueous complexation behavior of these hosts can be ascribed to the non-classical hydrophobic effect.[64–66] The non-classical hydrophobic effect derives from the cavity bound water molecules that do not possess a full complement of H-bonds that are released upon complexation. The entropic contributions to binding (−TΔS, kcal mol^{-1}) are presented for the host-drug complexes in the supplemental information. The −TΔS values are almost always positive (−TΔS [kcal mol^{-1}] for P5AS: −0.628 to +7.61; WP6: −0.756 to +3.99; P6AS +0.833 to +14.9; P7AS: −0.383 to +9.62), which indicates that the binding events are disfavored entropically. We surmise that restriction of conformational degrees of freedom of host and guest upon complexation more than offsets the changes in aqueous solvation of host and guest upon complexation. Given the large negative ΔH values observed for P6AS-drug complexes, and the well-known

Table 1. Binding constants (K_a, M^{-1}) and enthalpies (ΔH, kcal mol^{-1}) of complexation between the various hosts and drugs measured by direct or competitive ITC titrations at 298 K in 20-mM sodium phosphate-buffered H_2O at pH 7.4

Guest	P5AS	WP6	P6AS	P7AS	M1[50,58]	M2[50,58]
Meth	n.b.[d]	(1.72 ± 0.05) × 10^5[a] −7.75 ± 0.023	(9.90 ± 0.39) × 10^6[b] −10.4 ± 0.04 (2.17 ± 0.22) × 10^6[a] −8.53 ± 0.08 (PBS)	(2.03 ± 0.13) × 10^5[a] −6.86 ± 0.098	(1.47 ± 0.06) × 10^6−11.2 ± 0.02	(2.00 ± 0.10) × 10^6−10.0 ± 0.04
Fentanyl	(6.62 ± 0.45) × 10^5[a] −9.78 ± 0.115	(1.69 ± 0.06) × 10^6[a] −11.9 ± 0.051	(1.02 ± 0.03) × 10^8[c]−15.0 ± 0.052 (1.28 ± 0.057) × 10^7 −14.9 ± 0.054 (PBS)	(6.85 ± 0.44) × 10^6[f] −14.1 ± 0.131	(1.10 ± 0.40) × 10^7−20.9 ± 0.06	(7.60 ± 0.50) × 10^6−20.2 ± 0.07
Cocaine	n.b.[d]	n.b.[d]	(1.92 ± 0.06) × 10^6[a] −15.6 ± 0.047	n.b.[d]	(4.04 ± 0.39) × 10^5−11.0 ± 0.07	(5.21 ± 0.77) × 10^5−17.4 ± 0.46
Ketamine	(1.09 ± 0.14) × 10^5[a] −14.2 ± 0.635	n.b.[d]	(1.52 ± 0.25) × 10^5[a]−22.0 ± 1.02	(2.99 ± 0.09) × 10^5[a] −12.7 ± 0.078	(1.19 ± 0.21) × 10^4−6.95 ± 0.99	(3.70 ± 0.47) × 10^5 −13.6 ± 0.03
PCP	(2.51 ± 0.45) × 10^5[e] −6.74 ± 0.302	(9.01 ± 0.19) × 10^4[a] −8.64 ± 0.053	(5.85 ± 0.47) × 10^7 −12.4 ± 0.076	(1.08 ± 0.06) × 10^7[f] −12.4 ± 0.082	(6.25 ± 0.36) × 10^4−6.08 ± 0.13	(3.48 ± 0.20) × 10^5 −6.08 ± 0.07
Morphine	n.b.[d]	(4.15 ± 0.11) × 10^5[a] −11.7 ± 0.052	(1.36 ± 0.07) × 10^6[a]−12.9 ± 0.073	(8.85 ± 0.93) × 10^5[a] −15.3 ± 0.257	(6.29 ± 0.05) × 10^5−13.0 ± 0.18	(2.15 ± 0.81) × 10^6 −12.8 ± 0.73
Hydromorphone	n.b.[d]	(8.55 ± 0.16) × 10^4[a] −10.0 ± 0.056	(1.31 ± 0.04) × 10^6[a]−11.9 ± 0.042	(1.87 ± 0.26) × 10^6[a] −18.0 ± 0.290	(1.80 ± 0.03) × 10^5−11.20 ± 0.04	(6.80 ± 0.10) × 10^5 −12.1 ± 0.03
Oxycodone	n.b.[d]	n.b.[d]	(9.52 ± 0.36) × 10^4[a]−8.62 ± 0.097	(1.58 ± 0.13) × 10^6[a] −18.1 ± 0.162	(1.76 ± 0.04) × 10^5−11.9 ± 0.07	(1.16 ± 0.03) × 10^6 −14.8 ± 0.04
Heroin	(1.64 ± 0.24) × 10^4[a] −7.71 ± 0.73	(1.02 ± 0.05) × 10^5[a] −15.5 ± 0.2	(5.78 ± 0.02) × 10^5[a]−11.9 ± 0.11	(2.65 ± 0.13) × 10^6[g] −14.8 ± 0.1	(3.82 ± 0.65) × 10^5−14.0 ± 0.04	(5.29 ± 0.89) × 10^5 −17.7 ± 0.04
Mephedrone	(3.60 ± 0.13) × 10^5[a] −13.4 ± 0.1	(1.41 ± 0.06) × 10^6[a] −11.2 ± 0.0	(1.91 ± 0.19) × 10^7[f] −12.60 ± 0.11	(1.07 ± 0.05) × 10^5[a] −14.0 ± 0.2	(5.15 ± 0.42) × 10^5 −11.3 ± 0.16	(5.05 ± 0.29) × 10^6 −13.7 ± 0.07
MDMA	(7.29 ± 0.61) × 10^3[h] −12.9 ± 0.6	(4.50 ± 0.38) × 10^6[g] −11.7 ± 0.1	(3.92 ± 0.20) × 10^7[b] −13.30 ± 0.04	(1.08 ± 0.08) × 10^6[g] −8.88 ± 0.12	(1.13 ± 0.36) × 10^6 −15.0 ± 0.06	(1.00 ± 0.07) × 10^7 −17.7 ± 0.12

[a]Measured directly by ITC during the titration of host (0.1 mM) in the cell with guest (1 mM) in the syringe.
[b]Measured by competition with **14** = propane diammonium dichloride (0.15 mM).
[c]Measured by competition with **14** (1 mM).
[d]n.b. = no heat was evolved during the ITC titration of P6AS (100 μM) with drug (1 mM).
[e]Measured directly by ITC during the titration of host (0.05 mM) in the cell with guest (1 mM) in the syringe and the N sites is 2.
[f]Measured directly by ITC during the titration of host (0.01 mM) in the cell with guest (0.1 mM) in the syringe. –, not measured.
[g]Measured directly by ITC during the titration of host (0.025 mM) in the cell with guest (0.25 mM) in the syringe.
[h]Measured directly by ITC during the titration of host (0.25 mM) in the cell with guest (2.5 mM) in the syringe.

enthalpy-entropy compensation effects, the positive $-T\Delta S$ values are not surprising.[25,45]

The extensive dataset presented in Table 1 allows a discussion of the structural factors governing host-drug binding. We performed molecular modeling for uncomplexed P5AS, P6AS, and P7AS (supplemental information; Figure S60). We find that the average distance between the centroids of the *p*-phenylene walls and the centroid of the host cavity increases from P5AS (4.276 Å) to P6AS (5.244 Å) to P7AS (6.284 Å).[26] Accordingly, the larger hosts can accommodate larger and more bulky drugs as guests. It is well known from pillararene supramolecular chemistry that Pillar[5]arene binds well to *n*-alkane derivatives.[26] The cavity of P5AS is, therefore, too narrow to be a potent host for the drug panel and none of the complexes achieve sub-micromolar K_d values. Previously, we found that P6AS is a more potent host than WP6, particularly toward tertiary and quaternary ammonium ions.[56] This enhanced binding affinity cannot be attributed to general ion-ion interactions since both WP6 and P6AS have a net charge of −12 at neutral pH.[59] Accordingly, the differences between the binding affinity of WP6 and P6AS may arise due to the hydrophobic CH_2-linkers on WP6 partially invading its cavity, the higher charge density at the rim of the P6AS cavity due to the absence of the CH_2-linkers, differences in the solvation of the sulfate and carboxylate groups of P6AS versus WP6 or a combination of these and related effects. Experimentally, we find that P6AS is a more potent host than WP6 toward a specific drug by factors ranging from 3.3- to 649-fold. The narrower drugs (methamphetamine, fentanyl, mephedrone, and MDMA) are well accommodated by the cavity of P6AS with K_a values $\geq 10^7$ M^{-1}. Conversely, the larger P7AS host binds less strongly than P6AS to narrow drugs (meth: 49-fold; fentanyl: 15-fold) whereas P7AS displays comparable affinity to P6AS for drugs whose binding epitopes have larger cross-sectional areas (ketamine: 2.0-fold; PCP: 0.18-fold). Even bulkier drugs like oxycodone and heroin bind more strongly to the larger P7AS host by factors of 16- and 4.6-fold, respectively. Finally, a comparison with the acyclic CB[n]-type receptors M1 and M2 is warranted.[50,58] We find that P6AS is a more potent host toward the narrower guests than M1 (meth: 6.7-fold; fentanyl: 9.3-fold; mephedrone: 37-fold; MDMA: 35-fold) or M2 (meth: 5.0-fold; fentanyl: 13.4-fold; mephedrone: 3.8-fold; MDMA: 3.9-fold). The thermodynamic signatures of the formation of the P6AS-drug, M1-drug, and M2-drug complexes are similar, namely large negative ΔH values and positive $-T\Delta S$ values,[50,58] which originates from the release of cavity bound water molecules that do not possess a full complement of H-bonds upon complexation (e.g., non-classical hydrophobic effect).[64–66] Most significantly, the outstanding binding affinity of P6AS toward a variety of drugs (K_d: meth, 101 nM; fentanyl, 9.8 nM; PCP, 17.1 nM; mephedrone, 52.4 nM; MDMA, 25.5 nM) suggests that P6AS has great potential as a broad-spectrum sequestration agent for stimulants, narcotics, and hallucinogens.

In vitro cytotoxicity and *in vivo* MTD studies

In light of the outstanding binding affinity of P6AS toward the panel of drugs, we proceeded to evaluate the *in vitro* and *in vivo* biocompatibility of P6AS. First, we performed the 3-(4,5-dimethylthiazol-2-yl)-5-(3-carboxymethoxyphenyl)-2-(4-sulfophenyl)-2H-tetrazolium (MTS) and adenylate kinase (AK) release assays which measure cell viability and cell death, respectively. The MTS and AK release assays were performed using human kidney (HEK293 and American Type Culture Collection (ATCC) CRL-1573) and human liver (HepG2 and ATCC HB-8065) cells because compounds accumulate in the kidney and liver for metabolism and clearance (Figure 5). For the MTS assay, untreated cells were set to 100% viability, whereas for the AK release assay the data were normalized with respect to cells treated with distilled water (100% cell death).

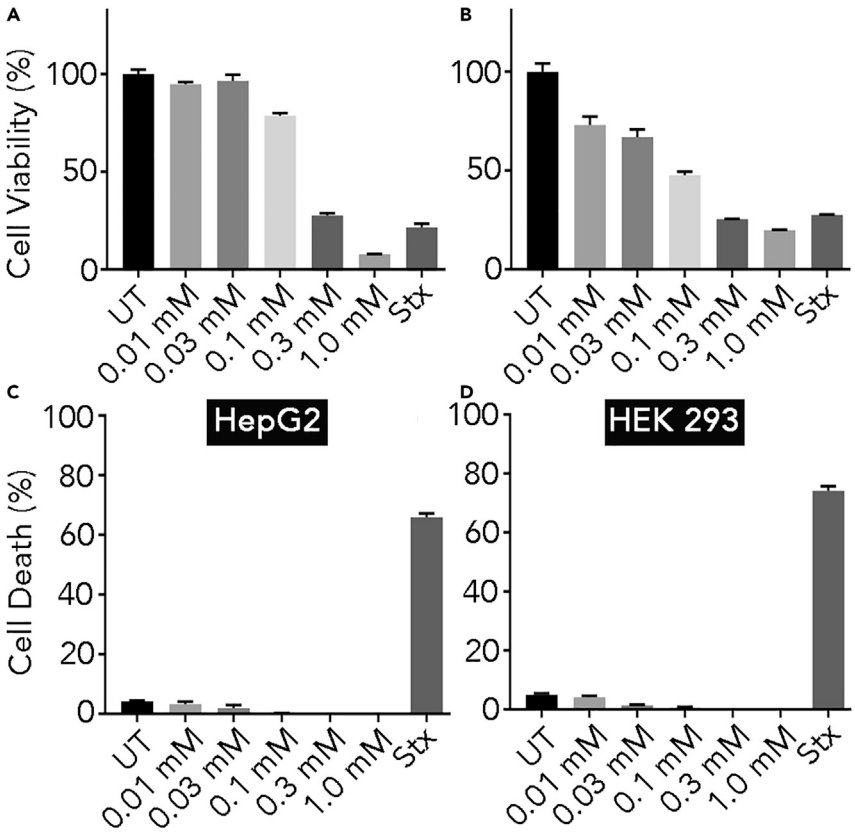

Figure 5. *In vitro* cytotoxicity assays performed for P6AS

(A and B) Cell viability assays (MTS) performed using P6AS at the stated concentrations for (A) HepG2, and (B) HEK293 cells after incubation for 24 h.

(C and D) Adenylate kinaseac (AK) release cell death assay performed using P6AS at the stated concentrations for (C) HepG2 and (D) HEK293 cells after incubation for 24 h. UT, untreated; Stx, staurosporine. Error bars show the average and the standard error of the mean (SEM).

Figures 5A and 5B show that cells treated with P6AS show a dose-dependent decrease in cell viability but maintain high cell tolerance up to 0.1 (HepG2) and 0.03 mM (HEK293). Figures 5C and 5D show that cells treated with up to 1.0 mM concentrations of P6AS do not undergo cell death according to the AK release assay relative to cells treated with distilled water and staurosporine as positive controls.

After having established an acceptable *in vitro* cytotoxicity profile, we decided to perform an *in vivo* MTD study. All animal studies were approved by the University of Maryland Animal Care and Use Committee (R-JAN-17-25 and R-AUG-18-42) and complied with the National Research Council Guide for the Care and Use of Laboratory Animals.[67] Female Swiss Webster mice (n = 15) were divided into three treatment groups (n = 5, P6AS doses: 136, 91, 45 mg kg^{-1}) and a control group (n = 5) that received PBS only. The mice were dosed via tail vein injection on days 0 and 2 (marked *) in a total volume of 0.150 mL. The mice were monitored every other day for changes in weight, behavior, and health status. Figure 6 shows that the weights of the animals receiving even the highest dose were comparable to those receiving PBS alone over the course of the study. However, animals receiving the highest dose (136 mg kg^{-1}) showed some adverse effects in the form of freeze ups and labored breathing; baseline behavior (e.g., PBS-like) was observed within 2–3 h after dosing. The animals treated with the lowest dose of P6AS

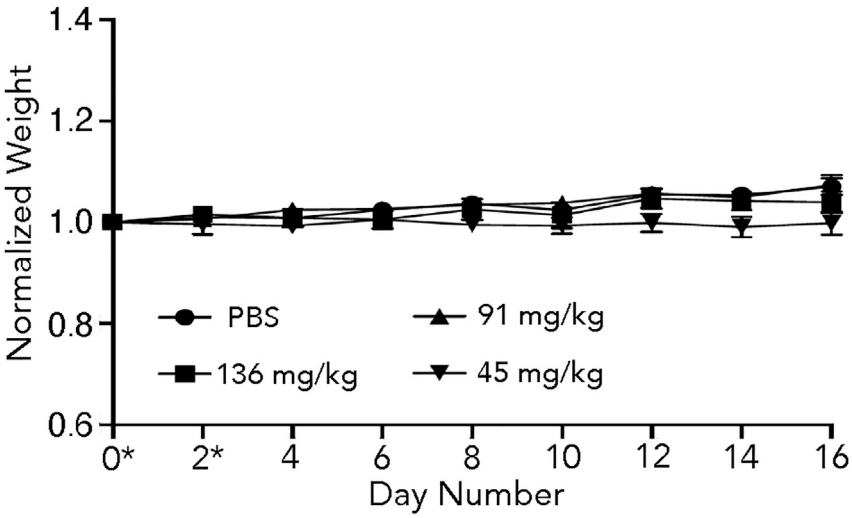

Figure 6. MTD study performed for P6AS

Female Swiss Webster mice (n = 5 per group) were dosed via tail vein injection (0.150 mL) on days 0 and 2 (denoted by *) with different concentrations of P6AS formulated in PBS or PBS alone. The normalized average weight change per study group is indicated. Error bars represent standard error of the mean (SEM).

(45 mg kg^{-1}) exhibited no adverse effects, and therefore, we designated 45 mg kg^{-1} as the no observed adverse effects level (NOAEL) for the planned *in vivo* efficacy studies.

P6AS does not inhibit the hERG ion channel

The hERG ion channel is involved in cardiac repolarization and is a voltage-gated potassium channel. Inhibition of the hERG ion channel can lead to potentially fatal cardiac malfunction due to the extension of electrical depolarization and repolarization of the heart ventricles. Developmental compounds are routinely screened early in the drug development process for hERG ion channel inhibition activity.[68] Figure 7 shows the results of an automated patch-clamp experiment (QPatch HTX) conducted using mammalian cells (HEK293) expressing the hERG ion channel using six different concentrations of P6AS (8 nM to 25 μM) and E-4031 as a positive control. The positive control (E-4031) exhibits a rapid increase in inhibition of the hERG ion channel at concentrations above 10 nM; the data can be fitted to determine an IC_{50} value of 26.7 nM for E-4031. In contrast, no significant change in hERG ion channel inhibition activity is seen for P6AS at concentrations up to 25 μM. Compounds with hERG ion channel inhibition IC_{50} values less than 100 nM are classified as highly potent whereas those greater than 10 μM are deemed to have little to no inhibitory activity.[69] Accordingly, since the IC_{50} for P6AS is >25 μM we deem it to have no significant hERG ion channel inhibitory activity, which encourages the further advancement of P6AS toward *in vivo* efficacy studies.

P6AS is not mutagenic according to the Ames fluctuation test

As a final prelude before proceeding to *in vivo* efficacy studies, the Ames fluctuation test was performed to determine the potential for genotoxicity of P6AS. Just like the Ames test, the Ames fluctuation test is a reverse mutation assay.[70,71] The Ames fluctuation test uses four different *S. typhimurium* strains (TA98, TA100, TA1535, and TA1537) that possess unique mutations within the histidine operon. Compounds that induce reverse mutations result in the growth of these strains in the absence of histidine which can be measured spectroscopically. The *S. typhimurium* strain

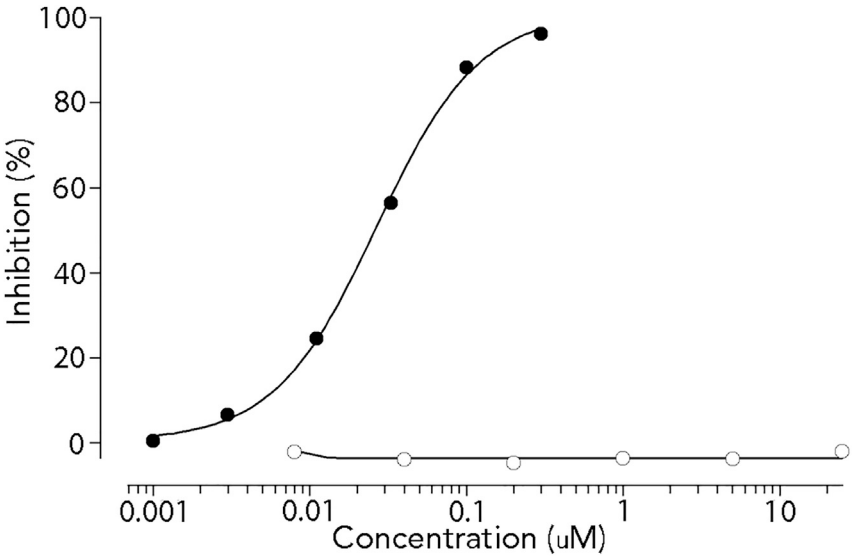

Figure 7. P6AS does not inhibit the hERG channel

The hERG assay was conducted using HEK293 stably transfected with hERG cDNA in an automated QPatch HTX patch-clamp study. Plot of mean hERG ion channel inhibition (%, n = 3–4) versus log concentration for E-4031 (●) and P6AS (o).

TA1535 contains a T to C missense mutation in the hisG gene (his G46) leading to a leucine to proline amino acid substitution; reverse mutation then allows identification of compounds that cause base pair mutations. In contrast, the TA1537 strain allows identification of compounds that induce a +1 frameshift mutation on the his C gene (his C3076). Similarly, the TA98 strain also detects +1 frameshift mutations on the his D gene (his D3052) but also features the pkM101 plasmid, which increases the sensitivity of TA98 to mutagenic compounds. Lastly, TA100 contains the same mutation as TA1535 and the pkM101 plasmid. Rat liver enzyme fractions (S9) are also used in the Ames fluctuation test to assess the potential mutagenicity of metabolites produced by the action of the liver enzymes on the test compound.

Initially, bacterial cytotoxicity assays were conducted with P6AS and the four tester strains (supplemental information; Figure S53) to document that P6AS was not cytotoxic toward the tester strains that would cause false negative results. Subsequently, the Ames fluctuation test was performed for P6AS along with suitable positive control compounds known to induce reverse mutation (2-aminoanthracene [2-AA], 9-aminoacridine [9-AA], quercetin, and streptozotocin), and the results are summarized in Table 2. For this purpose, the four tester strains were cultured overnight in media containing Davis Mingoli salts, D-glucose, D-biotin, and low level histidine at pH 7.0, which gave OD_{650} values in the 0.60–1.10 range. The cultures were then incubated with P6AS (5, 10, 50, 100 μM; n = 48) or the control compounds both with and without Arochlor-induced rat liver S9 fraction (0.2 mg mL^{-1}) for 96 h. Bromocresol purple is included as a colorimetric pH indicator that responds to the pH drop resulting from bacterial growth upon reverse mutation. After 96 h, the OD_{430} and OD_{570} values are measured, and the number of positive wells with $OD_{430}/OD_{570} \geq 1$ is determined as surrogate for reverse mutation. The significance of the number of positive wells in the treatment groups versus the control background group (no treatment) is calculated using the one-tailed Fisher's exact test and classified as follows: $p < 0.001$ (very strong positive, +++); $0.001 < p < 0.01$ (strong positive, ++); $0.01 < p < 0.05$ (weak positive, +); $p > 0.05$ (negative, –). An

Table 2. Results from the Ames fluctuation test conducted for P6AS

	TA98		TA100		TA1535		TA1537	
Treatment	−S9	+S9	−S9	+S9	−S9	+S9	−S9	+S9
Background	0/48	1/48	0/48	4/48	0/48	0/48	1/48	0/48
[P6AS] = 5 μM	0/48 –	2/48 –	0/48 –	0/48 –	0/48 –	0/48 –	0/48 –	1/48 –
[P6AS] = 10 μM	0/48 –	0/48 –	0/48 –	0/48 –	0/48 –	0/48 –	0/48 –	2/48 –
[P6AS] = 50 μM	0/48 –	0/48 –	0/48 –	1/48 –	1/48 –	0/48 –	0/48 –	0/48 –
[P6AS] = 100 μM	1/48 –	2/48 –	0/48 –	1/48 –	0/48 –	0/48 –	0/48 –	0/48 –
Streptozotocin	0/48 –	0/48 –	5/48 +	7/48 –	16/48 +++	24/48 +++	1/48 –	1/48 –
2-AA	0/48 –	13/48 +++	0/48 –	11/48 +	0/48 –	9/48 ++	0/48 –	6/48 +
Quercetin	5/48 +	10/48 +++	0/48 –	5/48 –	1/48 –	0/48 –	1/48 –	5/48 +
9-AA	0/48 –	0/48 –	0/48 –	2/48 –	0/48 –	0/48 –	24/48 +++	24/48 +++

examination of Table 2 shows that P6AS treatment did not result in any statistically significant increases in the number of positive wells relative to background. In contrast, the control compounds known to be genotoxic (streptozotocin, 2-AA, quercetin, and 9-AA) showed statistically significant increases in the number of positive wells in accord with their ability to induce reverse mutation. Accordingly, we conclude that P6AS does not statistically significantly increase the rate of reverse mutation and is not genotoxic.

P6AS functions as an *in vivo* sequestration agent that ameliorates the hyperlocomotion of mice treated with methamphetamine or fentanyl

Sequestration of methamphetamine

Based on the high affinity of P6AS toward methamphetamine and fentanyl and the favorable toxicology profile, we decided to perform *in vivo* efficacy tests (supplemental information; Figures S54–S59). For this purpose, we capitalized on the fact mice treated with methamphetamine (0.5 mg kg^{-1}) are known to exhibit hyperlocomotive effects[72,73] and that locomotion can be easily monitored by open-field tests.[74] A total of 8 adult male Swiss Webster mice were implanted with jugular catheters with head mounted ports as described previously.[46] All mice were habituated to the behavioral arena before testing. After a 10-day recovery period, on day 1, mice were placed in the open field to establish baseline locomotion levels before the treatments began. One session was conducted daily on days 2–7 using a semi-counterbalanced design where each mouse received one of six experimental treatments (PBS only; P6AS [35.7 mg kg^{-1}] only; methamphetamine [0.5 mg kg^{-1}, 0.022 mL of 0.89 mg mL^{-1} meth] only; a premixed solution of P6AS [35.7 mg kg^{-1}] and methamphetamine [0.5 mg kg^{-1}]; P6AS [35.7 mg kg^{-1}] followed 30 s later by methamphetamine [0.5 mg kg^{-1}] denoted as blocking; methamphetamine [0.5 mg kg^{-1}] followed 30 s later by P6AS [35.7 mg kg^{-1}] denoted as reversal). Locomotion values were obtained and analyzed using a one-way repeated measures ANOVA with Tukey-corrected pairwise post-hoc comparisons. Figure 8B shows a plot of locomotion count versus treatment group. A mixed effects analysis revealed a significant main effect of treatment ($F(5,35) = 7.116$, $p = 0.0001$) with Tukey-corrected post-hoc comparison showing a significant increase in locomotion counts for the methamphetamine group compared with all other treatment groups (p's < 0.05). Satisfyingly, there were no statistically significant differences in

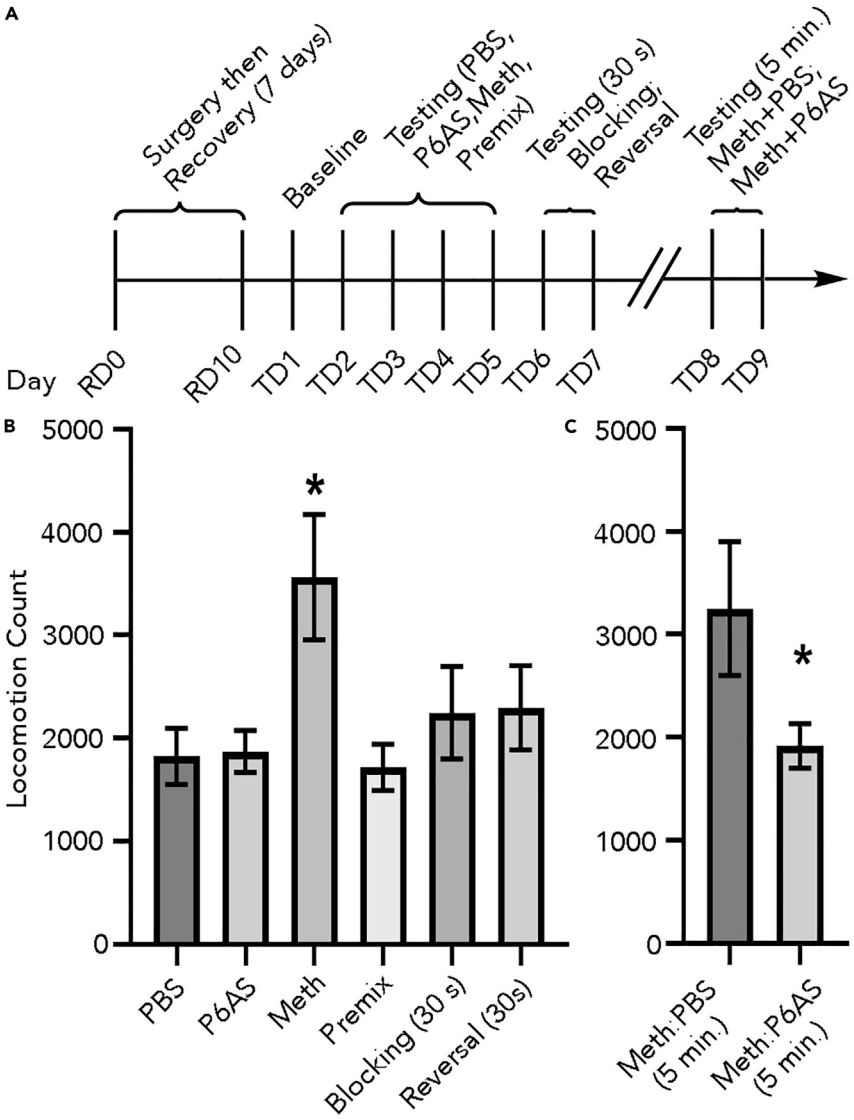

Figure 8. *In vivo* reversal of methamphetamine-induced hyperlocomotion by P6AS

(A) Testing schedule.

(B) Average locomotion counts for male Swiss Webster mice (n = 8; average weight ± SD: 39 ± 2.203 g) are plotted as a function of treatment. Treatment order was counterbalanced across days, and mice only received one treatment per day. Over 6 consecutive days of testing mice each received a single treatment of PBS (0.2 mL infused), P6AS only (P6AS; 35.7 mg kg^{-1}; 0.178 mL of 4 mM P6AS infused), methamphetamine only (meth; 0.5 mg/kg; 0.022 mL of 0.89 mg mL^{-1} meth infused), a premixed solution of P6AS and methamphetamine (premix; 35.7 mg kg^{-1} P6AS + 0.5 mg kg^{-1} meth infused), P6AS (35.7 mg kg^{-1}) followed by methamphetamine (0.5 mg kg^{-1}) administered 30 s later (denoted "blocking"), and methamphetamine (0.5 mg kg^{-1}) followed by P6AS (35.7 mg kg^{-1}) administered 30 s later (denoted "reversal"). Bars represent average locomotion counts. Error bars represent the SEM.

(C) 5-min reversal experiment: on days 8 and 9 mice (n = 8) received methamphetamine (0.5 mg kg^{-1}) followed by an infusion of PBS administered 5 min later (denoted meth:PBS [5 min]) or methamphetamine (0.5 mg kg^{-1}) followed by P6AS (35.7 mg kg^{-1}) administered 5 min later (denoted meth:P6AS [5 min]) in counterbalanced manner. Administration of P6AS 5 min after exposure to methamphetamine reduced hyperlocomotion (paired t test, $t(7) = 2.757$, $p = 0.0282$). Bars represent average locomotion counts. Error bars represent the standard error of the mean (SEM). The molar ratio of 35.7 mg kg^{-1} P6AS to 0.5 mg kg^{-1} methamphetamine is ≈7:1.

locomotion counts between the PBS group and the P6AS ($p > 0.9999$), premix ($p > 0.9999$), blocking 30 s ($p = 0.9481$), and reversal 30 s ($p = 0.9122$) treatment groups. These results strongly suggest that (1) pre-complexation of meth by P6AS in the syringe (Premix. group) effectively blocks the biological action of meth, (2) pre-circulating P6AS is able to capture meth in the bloodstream (e.g., blocking), and (3) treatment with P6AS 30 s after meth (reversal) effectively decreases the locomotion to levels that are statistically indistinguishable from PBS control group.

Despite these encouraging results, it is possible that the 30-s interval between methamphetamine administration and P6AS administration in the reversal group is too short to be ethologically relevant. To address this issue, we conducted a follow up experiment on days 8 and 9 where the same cohort of mice ($n = 8$) were administered either methamphetamine (0.5 mg kg^{-1}) followed by PBS 5 min later or methamphetamine (0.5 mg kg^{-1}) followed by P6AS (35.7 mg kg^{-1}) 5 min later in a counterbalanced manner before being placed in the open field (Figure 8C). We observed a significant decrease in locomotion counts in the meth + P6AS 5 min reversal condition relative to meth + PBS 5 min group (paired t test, $t(7) = 2.757$, $p = 0.0282$). Although not directly comparable from an experimental design perspective, it is important to note that locomotion levels in the meth + P6AS (5 min) reversal condition (Figure 8C) closely approximate those observed in control conditions from Figure 8B, whereas locomotion counts in the meth + PBS (min) group (Figure 8C) appear to approximate those observed with the methamphetamine only treatment (Figure 8B). Collectively, these findings establish that P6AS is capable of sequestering methamphetamine *in vivo* and reversing methamphetamine-induced hyperlocomotion, with little to no effect on the locomotor behavior of the animal itself.

Sequestration of fentanyl

P6AS binds extremely tightly to fentanyl in PBS ($K_a = 1.28 \times 10^7$ M^{-1}; $K_d = 78$ nM). Given the dramatic rise in overdose deaths due to fentanyl in the past decade that highlights the need for new and improved countermeasures,[57,75] we next explored the use of P6AS as an *in vivo* sequestrant for fentanyl. We selected a fentanyl dose of 0.1 mg kg^{-1} based on the literature reports.[76,77] Figures 9A–9C show plots of locomotion count versus treatment group that were conducted and analyzed for a cohort of male Swiss Webster mice ($n = 9$; avg. weight $\pm$ SD: 38.85 $\pm$ 2.1 g) in a manner analogous to that described above for methamphetamine. Figure 9A shows the results of the PBS alone, P6AS alone (35.8 mg kg^{-1}), and fentanyl (0.1 mg kg^{-1}) alone groups along with the premix, blocking (30 s), and reversal (30 s) treatment groups. Mixed effects analysis revealed a significant main effect of treatment ($F(5,40) = 23.50$, $p < 0.0001$) with Tukey-corrected post-hoc comparisons showing a significant increase in locomotion counts for treatment with fentanyl against all other treatment groups (p's < 0.05). In addition, there are no statistically significant differences in the locomotion counts between the PBS group and the P6AS ($p = 0.9103$), premix ($p = 0.9862$), blocking (30 s) ($p = 0.9985$), or reversal (30 s) ($p = 0.9966$) groups. Overall the results of Figure 9A show that P6AS is capable of sequestering fentanyl and modulates its hyperlocomotive effects with a 30-s inter-injection interval.

As with methamphetamine, we were concerned about the ethological relevance of the 30 s time point. Accordingly, we performed two additional experiments on the same cohort of 9 male Swiss Webster mice where the inter-injection intervals were extended. In the first reversal experiment (Figure 9B), mice were administered either fentanyl (0.1 mg kg^{-1}) followed by PBS 5 min later (denoted fentanyl:PBS [5 min]) or fentanyl (0.1 mg kg^{-1}) followed by P6AS (35.8 mg kg^{-1}) 5 min later (denoted fentanyl:P6AS [5 min]) in a counterbalanced manner before being placed in the open field.

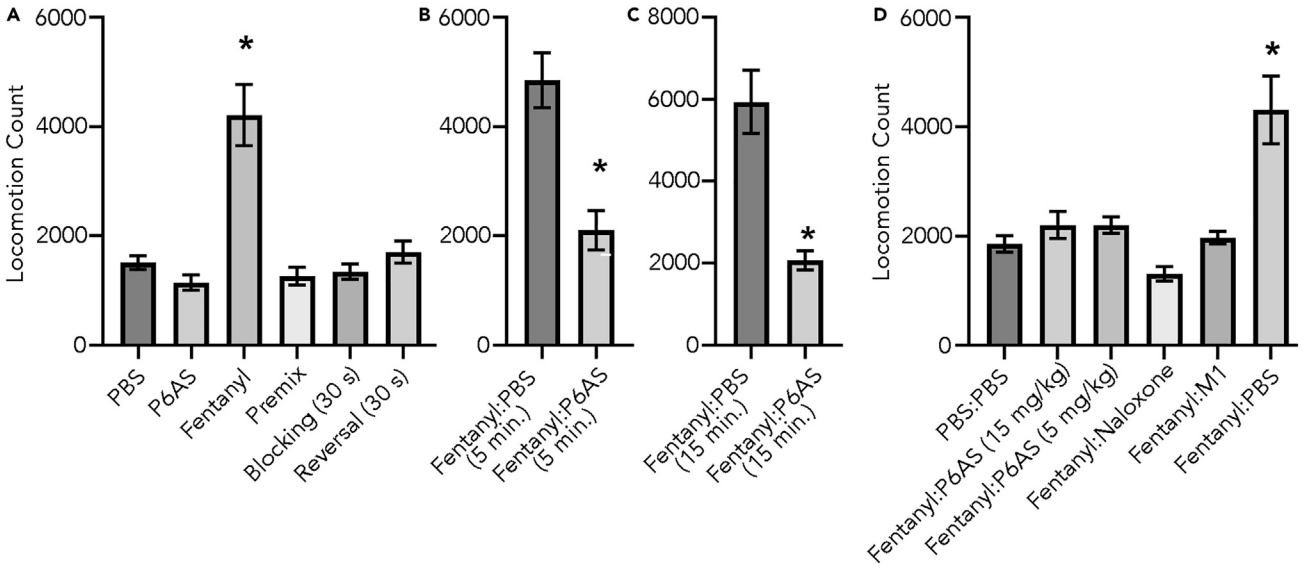

Figure 9. *In vivo* reversal of fentanyl induced hyperlocomotion by P6AS

(A) P6AS dose = 35.8 mg kg^{-1}. Average locomotion counts for male Swiss Webster mice (n = 9; avg. weight ± SD: 38.85 ± 2.1 g) are plotted as a function of treatment. All mice underwent an initial habituation to determine baseline locomotion levels before treatment. Following this baseline measure, treatment order was counterbalanced across days, and mice only received one treatment per day. Over 6 consecutive days of testing each mouse received a single treatment of PBS (0.2 mL infused), P6AS only (35.8 mg kg^{-1}; 0.178 mL of 4 mM P6AS infused), fentanyl only (0.1 mg/kg; 0.022 mL of 0.177 mg mL^{-1} fentanyl infused), a premixed solution of P6AS and fentanyl (premix; 35.8 mg kg^{-1} P6AS and 0.1 mg kg^{-1} fentanyl; 0.2 mL infused), P6AS (35.8 mg kg^{-1}) followed by fentanyl (0.1 mg kg^{-1}) administered 30 s later (denoted blocking 30 s), and fentanyl (0.1 mg kg^{-1}) followed by P6AS (35.8 mg kg^{-1}) administered 30 s later (denoted reversal 30 s).

(B) *In vivo* reversal of fentanyl induced hyperlocomotion by P6AS (35.8 mg kg^{-1}; 5-min inter-injection interval). Mice received either fentanyl (0.1 mg kg^{-1}; 0.022 mL of 0.177 mg mL^{-1} fentanyl infused) followed by PBS (0.178 mL infused) 5 min later (denoted fentanyl:PBS [5 min]) or fentanyl (0.1 mg kg^{-1}; 0.022 mL of 0.177 mg mL^{-1} fentanyl infused) followed by P6AS (35.8 mg kg^{-1}; 0.178 mL of 4 mM P6AS infused) administered 5 min later (denoted Fentantyl:P6AS [5 min]) before being placed into the behavioral box. Data analyzed using a paired t test.

(C) *In vivo* reversal of fentanyl induced hyperlocomotion by P6AS (35.8 mg kg^{-1}; 15-min inter-injection interval). Mice received either fentanyl (0.1 mg kg^{-1}; 0.022 mL of 0.177 mg mL^{-1} fentanyl infused) followed by PBS (0.178 mL infused) 15 min later (denoted fentanyl:PBS [15 min]) or fentanyl (0.1 mg kg^{-1}; 0.022 mL of 0.177 mg mL^{-1} fentanyl infused) followed by P6AS (35.8 mg kg^{-1}; 0.178 mL of 4 mM P6AS infused) administered 15 min later (denoted Fentantyl:P6AS [15 min]) before being placed into the behavioral box. Bars represent average locomotion counts. Error bars represent the SEM. Data analyzed using a paired t test. For (A)–(C), the molar ratio of P6AS:fentanyl is 68.3:1.

(D) *In vivo* reversal of fentanyl induced hyperlocomotion by P6AS (15 mg kg^{-1}; 7.66 μmol kg^{-1}), P6AS (5 mg kg^{-1}; 2.55 μmol kg^{-1}) M1 (11.81 mg kg^{-1}; 7.66 μmol kg^{-1}), or naloxone (NLX, 1 mg kg^{-1}; 2.75 μmol kg^{-1}). Average locomotion counts for male Swiss Webster mice (n = 11; average weight: 35.0 ± 1.42 g) are plotted as a function of treatment. Treatment order was counterbalanced across days, and mice only received one treatment per day. Mice were treated with either PBS (0.022 mL) or fentanyl (0.1 mg kg^{-1}, 0.022 mL of 0.1591 mg mL^{-1} fentanyl) followed 15 min later by 0.178 mL of a candidate countermeasure. The possible six treatments included PBS followed by PBS, fentanyl followed by P6AS (15 mg kg^{-1}; 0.178 mL of 1.507 mM P6AS), fentanyl followed by P6AS (5 mg kg^{-1}; 0.178 mL of 0.502 mM P6AS), fentanyl followed by naloxone (1 mg kg^{-1}; 0.178 mL of 1.591 mg mL^{-1} naloxone), fentanyl followed by M1 (11.81 mg kg^{-1}; 0.178 mM of 1.507 mM M1), or fentanyl followed by PBS (0.178 mL PBS). Bars represent average locomotion counts. Error bars represent the SEM. Dots represent counts for each mouse (n = 11). The molar ratio of P6AS:fentanyl is 28.6:1 for 15 mg kg^{-1} P6AS and 9.5:1 for 5 mg kg^{-1} P6AS.

We observed a significant decrease in locomotion when P6AS was given as countermeasure 5 min after fentanyl administration compared with locomotion counts when PBS was administered 5 min after fentanyl (paired t test, $t(8) = 6.208$, $p = 0.0003$; Figure 9B). For the second reversal experiment, we extended the inter-injection interval between fentanyl (0.1 mg kg^{-1}) administration and P6AS (35.8 mg kg^{-1}) or PBS treatment to 15 min (Figure 9C). As can be readily seen, P6AS is an effective at controlling to locomotion of the animals even when given 15 min after administration of fentanyl (paired t test, $t(8) = 5.050$, $p = 0.0010$). Excitingly, the overall results (Figures 9A–9C) establish that P6AS is capable of camouflaging (e.g., premix), capturing (e.g., blocking), and even reversing the hyperlocomotive effects of fentanyl up to 15 min after fentanyl administration due to the high-affinity nature of the P6AS-fentanyl complex.

Given the outstanding results presented above (Figures 9A–9C), we decided to explore whether lower doses of P6AS (15 and 5 mg kg^{-1}) at a 15-min inter-injection interval would remain efficacious at ameliorating the hyperlocomotion of animals dosed with fentanyl (0.1 mg kg^{-1}). In addition, we elected to include the Food and Drug Administration (FDA) approved countermeasure NLX and the experimental treatment M1, which has been shown[52] to sequester fentanyl *in vivo* by a PK strategy in rats. The results of this study using a new cohort of male Swiss Webster mice (n = 11; avg. weight: 35.0 ± 1.42 g) is shown in Figure 9D. As above, following surgery the mice were allowed to recover for 7 days and mice were habituated to the testing arena. Using a semi-counterbalanced design, each mouse received one of the six different treatments on each day of the study using a fixed inter-injection interval of 15 min. The six groups include two controls groups (PBS:PBS and fentanyl:PBS), two experimental groups (fentanyl:P6AS [15 mg kg^{-1}] and fentanyl:P6AS [5 mg kg^{-1}]) and two active comparator groups (fentanyl:naloxone [1 mg kg^{-1}][78] and fentanyl:M1). A mixed effects analysis of the data shown in Figure 9D revealed a significant main effect of treatment ($F(5,50) = 12.84$, $p < 0.0001$) with Tukey-corrected post-hoc comparison showing a significant increase in locomotion counts for the fentanyl:PBS group compared with the five other treatment groups (p's < 0.05). Importantly, no statistically significant differences (p's > 0.05) were observed between any other pair of treatment groups. For example, the locomotion counts for the PBS:PBS, fentanyl:P6AS (15 mg kg^{-1}; 7.66 μmol kg^{-1}), fentanyl:P6AS (5 mg kg^{-1}, 2.55 μmol kg^{-1}), and fentanyl:M1 (11.81 mg kg^{-1}, 7.66 μmol kg^{-1}) groups are indistinguishable (p's > 0.95) establishing that P6AS (15 or 5 mg kg^{-1}) is highly effective at reversing the hyperlocomotion of animals dosed with fentanyl. P6AS (7.66 μmol kg^{-1}) and M1 (7.66 μmol kg^{-1}) are similarly effective; both P6AS and M1 operate by a PK mechanism. Comparison of the fentanyl:naloxone group with PBS:PBS ($p = 0.7572$), fentanyl:P6AS (15 mg kg^{-1}) ($p = 0.2572$), fentanyl:P6AS (5 mg kg^{-1}) ($p = 0.2579$), and fentanyl:M1 ($p = 0.5861$) groups appear to trend toward significance which is perhaps not surprising because NLX operates by a different mechanism of action (PD). Even at the lowest dose of P6AS tested (5 mg kg^{-1}) the molar ratio of P6AS:fentanyl administered is 9.5:1, which suggests that further reductions in the dosage of P6AS may be possible.

Conclusions

In summary, we have reported improvements in the purification of P6AS that allows its isolation in 7.3 g batches. The binding of the panel of drugs of abuse toward P5AS, WP6, P6AS, and P7AS have been studied by a combination of ^{1}H NMR and ITC. Among these four hosts, we find that P6AS often displays the highest binding affinity toward a given drug. Of special note is the very tight binding exhibited by P6AS toward fentanyl (K_d = 9.8 nM), PCP (17.1 nM), MDMA (25.5 nM), mephedrone (52.4 nM), and methamphetamine (101 nM). P6AS displays good *in vitro* compatibility according to metabolic (MTS) and cell death (AK release) assays. According to *in vivo* MTD studies P6AS exhibits an NOAEL of 45 mg kg^{-1}. P6AS does not inhibit the hERG ion channel and is not mutagenic according to the Ames fluctuation test. *In vivo* efficacy tests showed that the hyperlocomotion of mice treated with methamphetamine (0.5 mg kg^{-1}) could be ameliorated by treatment with P6AS (35.7 mg kg^{-1}) up to 5 min later. Most significantly, we found that the hyperlocomotion observed for mice treated with fentanyl (0.1 mg kg^{-1}) could be reversed by treatment with P6AS up to 15 min later with P6AS doses as low as 5 mg kg^{-1}. The performance of P6AS (15 mg kg^{-1}; 7.66 μmol kg^{-1}) and M1 (7.66 μmol kg^{-1}) were not statistically significantly different and were comparable to treatment with NLX according to the open field tests. At the lowest dose studied, the P6AS:fentanyl molar ratio is 9.5:1, which,

given the outstanding binding affinity, suggests that further reductions in P6AS dose should be investigated. The combined inference of the results presented establish that P6AS is a potent *in vivo* reversal agent for methamphetamine and fentanyl and suggests that P6AS has translational potential as a broad-spectrum sequestration agent.

EXPERIMENTAL PROCEDURES

Resource availability

Lead contact

Further information and requests for resources or reagents should be directed to the lead contact, Lyle Isaacs (Lisaacs@umd.edu).

Materials availability

Subject to availability, samples of hosts will be made available following execution of a material transfer agreement.

Data and code availability

All data supporting the findings of this study are included within the article and its supplemental information and are also available from the authors upon request.

SUPPLEMENTAL INFORMATION

Supplemental information can be found online at https://doi.org/10.1016/j.chempr.2022.11.019.

ACKNOWLEDGMENTS

We thank the National Institutes of Health (GM132345) for financial support. M.S. thanks the NIH (T32 GM08021 and T32 AI089621) for support.

AUTHOR CONTRIBUTIONS

Conceptualization, L.I., V.B., M.R.R., and A.T.B.; investigation, A.T.B., W.X., C.-L.D., C.Z., M.S., D.K., and S.R.; writing—original draft, L.I. and A.T.B.; writing—review and editing, all authors; supervision, L.I., V.B., and M.R.R.; project administration, L.I.; funding acquisition, L.I., V.B., and M.R.R.

DECLARATION OF INTERESTS

The University of Maryland has filed a patent application covering the material in this publication with W.X. and L.I. named as inventors. L.I. is a consultant and scientific advisor and holds stock options in Clear Scientific (Cambridge, MA, USA).

Received: July 8, 2022
Revised: October 18, 2022
Accepted: October 23, 2022
Published: December 15, 2022

REFERENCES

1. https://www.drugabuse.gov/related-topics/trends-statistics#supplemental-references-for-economic-costs.
2. National drug threat assessment 2011. www.justice.gov/archive/ndic/pubs44/44849/44849p.pdf.
3. Behavioral health trends in the United States. https://www.samhsa.gov/data/sites/default/files/NSDUH-FRR1-2014/NSDUH-FRR1-2014.pdf.
4. Gorelick, D.A. (2012). Pharmacokinetic strategies for treatment of drug overdose and addiction. Future Med. Chem. *4*, 227–243.
5. Rzasa Lynn, R., and Galinkin, J.L. (2018). Naloxone dosage for opioid reversal: current evidence and clinical implications. Ther. Adv. Drug Saf. *9*, 63–88.
6. Moss, R.B., and Carlo, D.J. (2019). Higher doses of naloxone are needed in the synthetic opioid era. Subst. Abuse Treat. Prev. Policy *14*, 6.
7. Zhan, C.G., Zheng, F., and Landry, D.W. (2003). Fundamental reaction mechanism for cocaine

hydrolysis in human butyrylcholinesterase. J. Am. Chem. Soc. *125*, 2462–2474.

8. Zheng, F., Yang, W., Ko, M.C., Liu, J., Cho, H., Gao, D., Tong, M., Tai, H.H., Woods, J.H., and Zhan, C.G. (2008). Most efficient cocaine hydrolase designed by virtual screening of transition states. J. Am. Chem. Soc. *130*, 12148–12155.

9. Shram, M.J., Cohen-Barak, O., Chakraborty, B., Bassan, M., Schoedel, K.A., Hallak, H., Eyal, E., Weiss, S., Gilgun-Serki, Y., Sellers, E.M., et al. (2015). Assessment of pharmacokinetic and pharmacodynamic interactions between albumin-fused mutated butyrylcholinesterase and intravenously administered cocaine in recreational cocaine users. J. Clin. Psychopharmacol. *35*, 396–405.

10. Kosten, T.R., Domingo, C.B., Shorter, D., Orson, F., Green, C., Somoza, E., Sekerka, R., Levin, F.R., Mariani, J.J., Stitzer, M., et al. (2014). Vaccine for cocaine dependence: A randomized double-blind placebo-controlled efficacy trial. Drug Alcohol Depend. *140*, 42–47.

11. Stevens, M.W., Henry, R.L., Owens, S.M., Schutz, R., and Gentry, W.B. (2014). First human study of a chimeric anti-methamphetamine monoclonal antibody in healthy volunteers. mAbs *6*, 1649–1656.

12. Bremer, P.T., Kimishima, A., Schlosburg, J.E., Zhou, B., Collins, K.C., and Janda, K.D. (2016). Combatting synthetic designer opioids: A conjugate vaccine ablates lethal doses of fentanyl class drugs. Angew. Chem. Int. Ed. Engl. *55*, 3772–3775.

13. Collins, K.C., Schlosburg, J.E., Bremer, P.T., and Janda, K.D. (2016). Methamphetamine vaccines: improvement through hapten design. J. Med. Chem. *59*, 3878–3885.

14. Eubanks, L.M., Blake, S., Natori, Y., Ellis, B., Bremer, P.T., and Janda, K.D. (2021). A highly efficacious carfentanil vaccine that blunts opioid-induced antinociception and respiratory depression. ACS Chem. Biol. *16*, 277–282.

15. Deng, C.-L., Murkli, S.L., and Isaacs, L.D. (2020). Supramolecular hosts as in vivo sequestration agents for pharmaceuticals and toxins. Chem. Soc. Rev. *49*, 7516–7532.

16. Yin, H., Zhang, X., Wei, J., Lu, S., Bardelang, D., and Wang, R. (2021). Recent advances in supramolecular antidotes. Theranostics *11*, 1513–1526.

17. Cram, D.J. (1988). The design of molecular Hosts, Guests, and Their Complexes (Nobel Lecture). Angew. Chem. Int. Ed. Engl. *27*, 1009–1020.

18. Lehn, J.-M. (1988). Supramolecular chemistry – scope and perspectives: molecules, supermolecules, and Molecular Devices (Nobel lecture). Angew. Chem. Int. Ed. Engl. *27*, 89–112.

19. Pedersen, C.J. (1988). The discovery of crown ethers (Nobel lecture). Angew. Chem. Int. Ed. Engl. *27*, 1021–1027.

20. Stoddart, J.F. (2017). Mechanically interlocked molecules (MIMs)—molecular shuttles, switches, and machines. Angew. Chem. Int. Ed. Engl. *56*, 11094–11125.

21. Gutsche, C.D. (1983). Calixarenes. Acc. Chem. Res. *16*, 161–170.

22. Diederich, F. (1988). Complexation of neutral molecules by cyclophane Hosts. Angew. Chem. Int. Ed. Engl. *27*, 362–386.

23. Böhmer, V. (1995). Calixarenes macrocycles with (almost) unlimited possibilities. Angew. Chem. Int. Ed. Engl. *34*, 713–745.

24. Rajewski, R.A., and Stella, V.J. (1996). Pharmaceutical applications of cyclodextrins. 2. In vivo drug delivery. J. Pharm. Sci. *85*, 1142–1169.

25. Rekharsky, M.V., and Inoue, Y. (1998). Complexation thermodynamics of cyclodextrins. Chem. Rev. *98*, 1875–1918.

26. Xue, M., Yang, Y., Chi, X., Zhang, Z., and Huang, F. (2012). Pillararenes, A new class of macrocycles for supramolecular chemistry. Acc. Chem. Res. *45*, 1294–1308.

27. Barrow, S.J., Kasera, S., Rowland, M.J., del Barrio, J., and Scherman, O.A. (2015). Cucurbituril-based molecular recognition. Chem. Rev. *115*, 12320–12406.

28. Ogoshi, T., Yamagishi, T.-A., and Nakamoto, Y. (2016). Pillar-shaped macrocyclic Hosts Pillar[n]arenes: New Key Players for Supramolecular Chemistry. Chem. Rev. *116*, 7937–8002.

29. Murray, J., Kim, K., Ogoshi, T., Yao, W., and Gibb, B.C. (2017). The aqueous supramolecular chemistry of cucurbit[n]urils, pillar[n]arenes and deep-cavity cavitands. Chem. Soc. Rev. *46*, 2479–2496.

30. Ghale, G., and Nau, W.M. (2014). Dynamically analyte-responsive macrocyclic host-fluorophore systems. Acc. Chem. Res. *47*, 2150–2159.

31. Meadows, M.K., and Anslyn, E.V. (2016). Three tales of supramolecular analytical chemistry. Macrocyclic Supramol. Chem. 92–126.

32. McCune, J.A., Mommer, S., Parkins, C.C., and Scherman, O.A. (2020). Design principles for aqueous interactive materials: lessons from small molecules and stimuli-responsive systems. Adv. Mater. *32*, e1906890.

33. Kassem, S., van Leeuwen, T., Lubbe, A.S., Wilson, M.R., Feringa, B.L., and Leigh, D.A. (2017). Artificial molecular motors. Chem. Soc. Rev. *46*, 2592–2621.

34. Roland, F.M., and Smith, B.D. (2019). Probes for medical imaging. Supramol. Chem. Water, 501–524.

35. Zhang, H., Ma, X., Nguyen, K.T., and Zhao, Y. (2013). Biocompatible pillararene-assembly-based carriers for dual bioimaging. ACS Nano *7*, 7853–7863.

36. Guo, D.S., and Liu, Y. (2014). Supramolecular chemistry of p-Sulfonatocalix[n]arenes and its biological applications. Acc. Chem. Res. *47*, 1925–1934.

37. Webber, M.J., and Langer, R. (2017). Drug delivery by supramolecular design. Chem. Soc. Rev. *46*, 6600–6620.

38. Xiao, T., Qi, L., Zhong, W., Lin, C., Wang, R., and Wang, L. (2019). Stimuli-responsive nanocarriers constructed from pillar[n]arene-based supra-amphiphiles. Mater. Chem. Front. *3*, 1973–1993.

39. Stella, V.J., and Rajewski, R.A. (1997). Cyclodextrins: their future in drug formulation and delivery. Pharm. Res. *14*, 556–567.

40. Adam, J.M., Bennett, D.J., Bom, A., Clark, J.K., Feilden, H., Hutchinson, E.J., Palin, R., Prosser, A., Rees, D.C., Rosair, G.M., et al. (2002). Cyclodextrin-derived host molecules as reversal agents for the neuromuscular blocker rocuronium bromide: synthesis and structure-activity relationships. J. Med. Chem. *45*, 1806–1816.

41. Bom, A., Bradley, M., Cameron, K., Clark, J.K., Van Egmond, J., Feilden, H., MacLean, E.J., Muir, A.W., Palin, R., Rees, D.C., et al. (2002). A novel concept of reversing neuromuscular block: chemical encapsulation of rocuronium bromide by a cyclodextrin-based synthetic host. Angew. Chem. Int. Ed. Engl. *41*, 266–270.

42. Wang, K., Guo, D.-S., Zhang, H.-Q., Li, D., Zheng, X.-L., and Liu, Y. (2009). Highly effective binding of viologens by p-sulfonatocalixarenes for the treatment of viologen poisoning. J. Med. Chem. *52*, 6402–6412.

43. Liu, S., Ruspic, C., Mukhopadhyay, P., Chakrabarti, S., Zavalij, P.Y., and Isaacs, L. (2005). The cucurbit[n]uril family: prime components for self-sorting systems. J. Am. Chem. Soc. *127*, 15959–15967.

44. Assaf, K.I., and Nau, W.M. (2015). Cucurbiturils: from synthesis to high-affinity binding and catalysis. Chem. Soc. Rev. *44*, 394–418.

45. Shetty, D., Khedkar, J.K., Park, K.M., and Kim, K. (2015). Can we beat the biotin–avidin pair?: cucurbit[7]uril-based ultrahigh affinity host-guest complexes and their applications. Chem. Soc. Rev. *44*, 8747–8761.

46. Murkli, S., Klemm, J., Brockett, A.T., Shuster, M., Briken, V., Roesch, M.R., and Isaacs, L. (2021). In vitro and in vivo sequestration of phencyclidine by Me4Cucurbit[8]uril**. Chemistry *27*, 3098–3105.

47. Chen, H., Chan, J.Y.W., Li, S., Liu, J.J., Wyman, I.W., Lee, S.M.Y., Macartney, D.H., and Wang, R. (2015). In vivo reversal of general anesthesia by cucurbit[7]uril with zebrafish models. RSC Adv. *5*, 63745–63752.

48. Zhang, X., Cheng, Q., Li, L., Shangguan, L., Li, C., Li, S., Huang, F., Zhang, J., and Wang, R. (2019). Supramolecular therapeutics to treat the side effects induced by a depolarizing neuromuscular blocking agent. Theranostics *9*, 3107–3121.

49. Zhang, X., Xu, X., Li, S., Li, L., Zhang, J., and Wang, R. (2019). A synthetic receptor as a specific antidote for paraquat poisoning. Theranostics *9*, 633–645.

50. Ganapati, S., Grabitz, S.D., Murkli, S., Scheffenbichler, F., Rudolph, M.I., Zavalij, P.Y., Eikermann, M., and Isaacs, L. (2017). Molecular containers bind drugs of abuse in vitro and reverse the hyperlocomotive effect of methamphetamine in rats. Chembiochem *18*, 1583–1588.

51. Ganapati, S., and Isaacs, L. (2018). Acyclic cucurbit[n]uril-type receptors: preparation, molecular recognition properties and

biological applications. Isr. J. Chem. *58*, 250–263.

52. Thevathasan, T., Grabitz, S.D., Santer, P., Rostin, P., Akeju, O., Boghosian, J.D., Gill, M., Isaacs, L., Cotten, J.F., and Eikermann, M. (2020). Calabadion 1 selectively reverses respiratory and central nervous system effects of fentanyl in a rat model. Br. J. Anaesth. *125*, e140–e147.

53. Sathiyajith, C., Shaikh, R.R., Han, Q., Zhang, Y., Meguellati, K., and Yang, Y.W. (2017). Biological and related applications of pillar[n]arenes. Chem. Commun. (Camb) *53*, 677–696.

54. Chai, Y., Chen, L., Zhang, Y., Zhao, L., Meng, Z., Chen, J., Li, C., and Meng, Q. (2022). Reversing neuromuscular blocking agent decamethonium by carboxylatopillar[6]arene based on host-guest encapsulation. Chin. Chem. Lett. *33*, 3003–3006.

55. Li, C., Xie, Z., Chen, Q., Zhang, Y., Chu, Y., Guo, Q., Zhou, W., Zhang, Y., Liu, P., Chen, H., et al. (2020). Supramolecular hunter stationed on red blood cells for detoxification based on specific molecular recognition. ACS Nano *14*, 4950–4962.

56. Xue, W., Zavalij, P.Y., and Isaacs, L. (2020). Pillar[n]MaxQ: A new high affinity Host Family for Sequestration in Water. Angew. Chem. Int. Ed. Engl. *59*, 13313–13319.

57. Centers for Disease Control and Prevention (2019). Surveillance Report of Drug-Related Risks and Outcomes. https://www.cdc.gov/drugoverdose/pdf/pubs/2019-cdc-drug-surveillance-report.pdf.

58. DiMaggio, D., Brockett, A.T., Shuster, M., Murkli, S., Zhai, C., King, D., O'Dowd, B., Cheng, M., Brady, K., Briken, V., et al. (2022). Anthracene-walled acyclic CB[n] receptors: in vitro and in vivo binding properties toward drugs of abuse. ChemMedChem *17*, e202200046.

59. Deng, C.-L., Cheng, M., Zavalij, P.Y., and Isaacs, L. (2022). Thermodynamics of pillararene·guest complexation: blinded dataset for the SAMPL9 challenge. New J. Chem. *46*, 995–1002.

60. Liu, Y., Zhou, F., Yang, F., and Ma, D. (2019). Carboxylated pillar[n]arene (n = 5–7) host molecules: high affinity and selective binding in water. Org. Biomol. Chem. *17*, 5106–5111.

61. Wiseman, T., Williston, S., Brandts, J.F., and Lin, L.-N. (1989). Rapid measurement of binding constants and heats of binding using a new titration calorimeter. Anal. Biochem. *179*, 131–137.

62. Broecker, J., Vargas, C., and Keller, S. (2011). Revisiting the optimal c value for isothermal titration calorimetry. Anal. Biochem. *418*, 307–309.

63. Velazquez-Campoy, A., and Freire, E. (2006). Isothermal titration calorimetry to determine association constants for high-affinity ligands. Nat. Protoc. *1*, 186–191.

64. Persch, E., Dumele, O., and Diederich, F. (2015). Molecular recognition in chemical and biological systems. Angew. Chem. Int. Ed. Engl. *54*, 3290–3327.

65. Biedermann, F., Nau, W.M., and Schneider, H.J. (2014). The hydrophobic effect revisited-studies with supramolecular complexes imply high-energy water as a noncovalent driving force. Angew. Chem. Int. Ed. Engl. *53*, 11158–11171.

66. King, D., Wilson, C.R., Herron, L., Deng, C.L., Mehdi, S., Tiwary, P., Hof, F., and Isaacs, L. (2022). Molecular recognition of methylated amino acids and peptides by Pillar[6]MaxQ. Org. Biomol. Chem. *20*, 7429–7438.

67. National Research Council (US) Committee for the Update of the Guide for the Care and Use of Laboratory Animals (2011). Guide for the Care and Use of Laboratory Animals (National Academies Press).

68. Bell, D.C., and Fermini, B. (2021). Use of automated patch clamp in cardiac safety assessment: past, present and future perspectives. J. Pharmacol. Toxicol. Methods *110*, 107072.

69. Roche, O., Trube, G., Zuegge, J., Pflimlin, P., Alanine, A., and Schneider, G. (2002). A virtual screening method for prediction of the HERG potassium channel liability of compound libraries. Chembiochem *3*, 455–459.

70. Bridges, B.A. (1980). The fluctuation test. Arch. Toxicol. *46*, 41–44.

71. Kamber, M., Flückiger-Isler, S., Engelhardt, G., Jaeckh, R., and Zeiger, E. (2009). Comparison of the Ames II and traditional Ames test responses with respect to mutagenicity, strain specificities, need for metabolism and correlation with rodent carcinogenicity. Mutagenesis *24*, 359–366.

72. Sharp, A.L., Varela, E., Bettinger, L., and Beckstead, M.J. (2015). Methamphetamine self-Administration in Mice Decreases GIRK Channel-Mediated Currents in Midbrain Dopamine Neurons. Int. J. Neuropsychopharmacol. *18*, 1–10.

73. Singh, R.A.K., Kosten, T.A., Kinsey, B.M., Shen, X., Lopez, A.Y., Kosten, T.R., and Orson, F.M. (2012). Dose-dependent changes in the locomotor responses to methamphetamine in BALB/c mice: low doses induce hypolocomotion. Pharmacol. Biochem. Behav. *103*, 230–236.

74. Walsh, R.N., and Cummins, R.A. (1976). The open-field test: A critical review. Psychol. Bull. *83*, 482–504.

75. https://www.drugabuse.gov/about-nida/legislative-activities/testimony-to-congress/2021/the-overdose-crisis-proposal-to-combat-illicit-fentanyl.

76. Bryant, C.D., Roberts, K.W., Culbertson, C.S., Le, A., Evans, C.J., and Fanselow, M.S. (2009). Pavlovian conditioning of multiple opioid-like responses in mice. Drug Alcohol Depend. *103*, 74–83.

77. Moussawi, K., Ortiz, M.M., Gantz, S.C., Tunstall, B.J., Marchette, R.C.N., Bonci, A., Koob, G.F., and Vendruscolo, L.F. (2020). Fentanyl vapor self-administration model in miceto study opioid addiction. Sci. Adv. *6*, eabc0413.

78. Yang, W., Law, P.Y., Guo, X., and Loh, H.H. (2003). In vivo activation of a mutant-opioid receptor by antagonist: future direction for opiate pain treatment paradigm that lacks undesirable side effects. Proc. Natl. Acad. Sci. USA *100*, 2117–2121.